Acta Crystallographica Section F
Structural Biology and Crystallization Communications
ISSN 1744-3091

Crystallization and preliminary characterization of the *Thermus thermophilus* RNA helicase Hera C-terminal domain

Markus G. Rudolph,[a]* Julia G. Wittmann[a] and Dagmar Klostermeier[b]

[a]Department of Molecular Structural Biology, Institute for Microbiology and Genetics, Georg-August-Universität, Justus-von-Liebig Weg 11, 37077 Göttingen, Germany, and [b]Department of Biophysical Chemistry, Biozentrum, University of Basel, Klingelbergstrasse 50/70, 4056 Basel, Switzerland

Correspondence e-mail: mrudolp2@gwdg.de

Received 18 September 2008
Accepted 18 December 2008

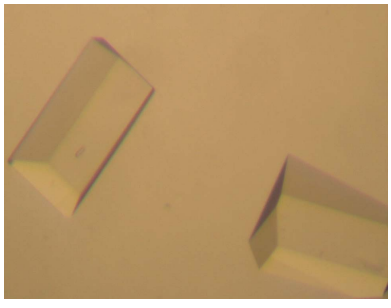

Heat-resistant RNA-dependent ATPase (Hera) from *Thermus thermophilus* is a DEAD-box RNA helicase. Two constructs encompassing the second RecA-like domain and the C-terminal domain of Hera were overproduced in *Escherichia coli* and purified to homogeneity. Single crystals of both Hera constructs were obtained in three crystal forms. A tetragonal crystal form belonged to space group $P4_12_12$, with unit-cell parameters $a = 65.5$, $c = 153.0$ Å, and contained one molecule per asymmetric unit. Two orthorhombic forms belonged to space group $P2_12_12_1$, with unit-cell parameters $a = 62.8$, $b = 70.9$, $c = 102.3$ Å (form I) and $a = 41.6$, $b = 67.6$, $c = 183.5$ Å (form II). Both orthorhombic forms contained two molecules per asymmetric unit. All crystals diffracted X-rays to beyond 3 Å resolution, but the tetragonal data sets displayed high Wilson B values and high mean $|E^2 - 1|$ values, indicating potential disorder and anisotropy. The tetragonal crystal was phased by MAD using a single selenium site.

1. Introduction

Structural changes in RNA or RNA–protein complexes during (viral) replication, transcription, mRNA splicing, translation and ribosome assembly are mediated by RNA helicases (Pyle, 2008). These enzymes use the chemical energy of ATP to reorganize their substrates. The DEAD-box helicases constitute the largest family within helicase superfamily 2 and are found in all kingdoms of life. RNA helicases are organized as two RecA-like domains that carry signature motifs for ATP and RNA binding and RNA remodelling. In addition, many helicases contain flanking C-terminal domains that contribute to specific or nonspecific high-affinity RNA binding (Diges & Uhlenbeck, 2001; Tsu *et al.*, 2001; Kossen *et al.*, 2002; Mohr *et al.*, 2008). It has been suggested that these C-terminal domains may also position the RNA substrate with respect to the helicase core (Mohr *et al.*, 2008; Halls *et al.*, 2007; Huang *et al.*, 2005). The opening and closing of a cleft formed by the RecA domains has been found to be crucial for unwinding (Theissen *et al.*, 2008). Thus, nucleic acid binding and release cycles require large conformational changes in RNA helicases, rendering them flexible and difficult to crystallize in the apo form. The crystal structures of several RNA helicase–RNA complexes in the closed conformation have been determined (Sengoku *et al.*, 2006; Andersen *et al.*, 2006; Bono *et al.*, 2006) and show pronounced similarity, while the open forms of the helicases tend to differ more strongly from each other. Structural information on ancillary RNA-binding domains is limited to the isolated C-terminal domain of the DEAD-box helicase YxiN, which is involved in ribosome biogenesis. The YxiN C-terminal domain forms a classical RNA-recognition motif that mediates specific binding to a hairpin in the 23S ribosomal RNA (Wang *et al.*, 2006; Kossen *et al.*, 2002).

The heat-resistant RNA-dependent ATPase Hera was cloned from *Thermus thermophilus* and some of its biochemical properties have been assessed (Linden *et al.*, 2008; Morlang *et al.*, 1999). Hera contains a C-terminal domain that bears no sequence similarity to the C-terminal domains of other RNA helicases. However, it contains a short sequence with a weak similarity to a conserved motif in the

RNase P protein component. It has been shown that the C-terminal domain of Hera, but not the putative RNase P motif, is required for RNA binding (Linden *et al.*, 2008). In addition, gel-permeation chromatography has shown that Hera forms a stable dimer in solution (Linden *et al.*, 2008), raising the question as to how dimerization might be linked to RNA binding and helicase function.

To begin answering these questions, the gene coding for *T. thermophilus* HB27 Hera was cloned from genomic DNA (Linden *et al.*, 2008) and the protein was recombinantly produced in *Escherichia coli*. Full-length Hera proved resilient to crystallization, necessitating the generation of the N- and C-terminal domains. The crystal structure of the N-terminal Hera domain in complex with the unusual ligand AMP has been determined previously (Rudolph *et al.*, 2006), but for a complete picture the structure of the C-terminal domain is required. We crystallized two constructs of the C-terminal domain of Hera in three crystal forms and employed SeMet MAD phasing using a single selenium site to generate initial electron-density maps.

2. Methods

2.1. Protein purification and crystallization

The Hera gene was cloned from genomic DNA of *T. thermophilus* HB27 and the protein was overproduced in *E. coli*. Purification of full-length Hera is described in detail elsewhere (Linden *et al.*, 2008). For the production of C-terminal Hera constructs, two DNA fragments encoding Hera residues 208–510 and 208–419 were generated by PCR and cloned into the *Nco*I/*Bam*HI sites of pET28a (Novagen), thereby removing the His_6 tag of the vector. The plasmid coding for Hera_208–510 was transformed into *E. coli* BL21 (DE3) RIL

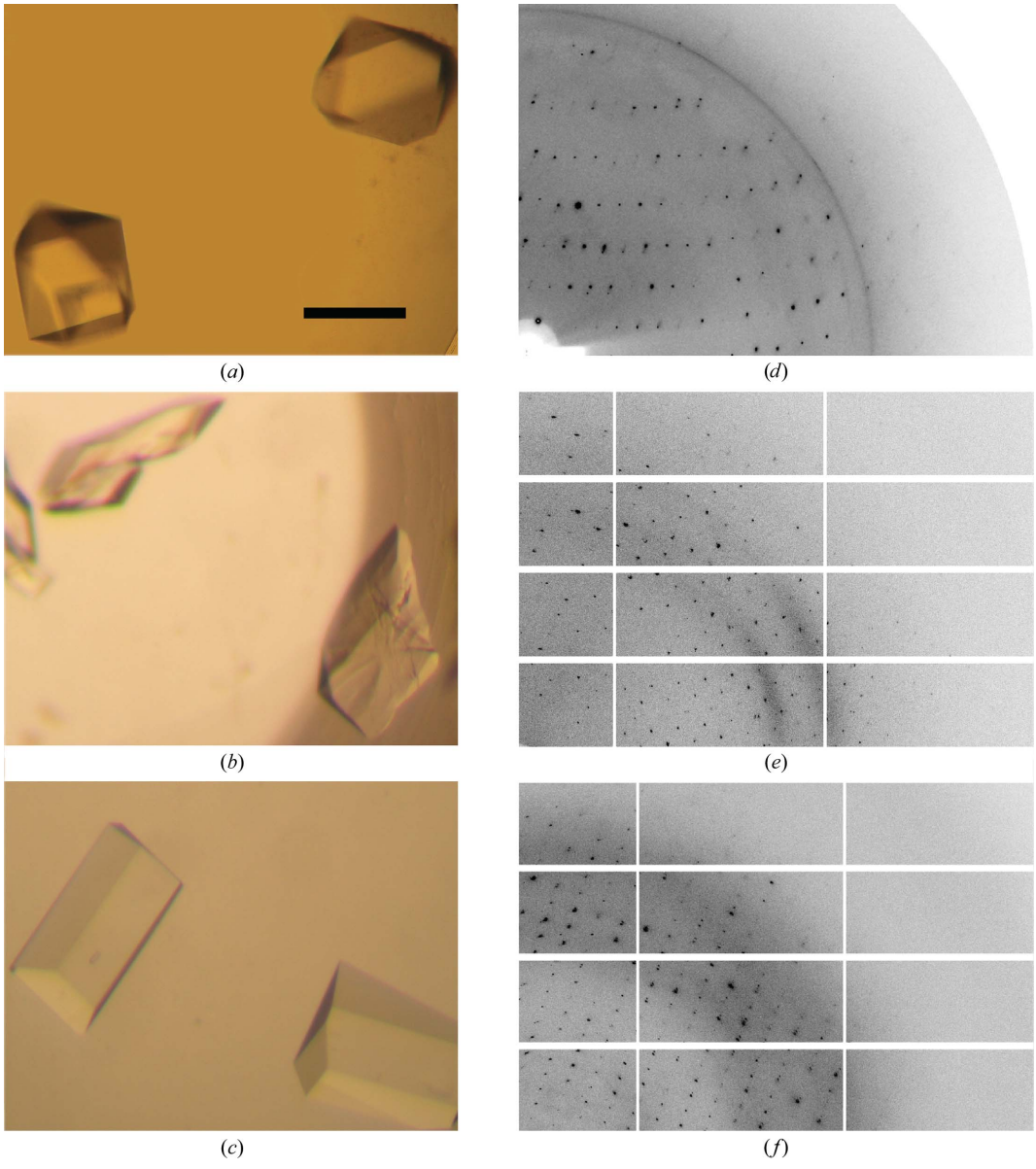

Figure 1
(*a*) Tetragonal Hera_208–510 crystals. (*b*) Orthorhombic Hera_208–419 crystals (form I). (*c*) Orthorhombic Hera_208–419 crystals (form II). The scale bar in (*a*) is 0.2 mm and applies to all crystal images. (*d*), (*e*) and (*f*) show diffraction patterns of the crystals in (*a*), (*b*) and (*c*), respectively. Resolution limits: (*d*) 3.7 Å (top) and 2.6 Å (right); (*e*) 3.0 Å (top) and 2.4 Å (right); (*f*) 3.0 Å (top) and 2.0 Å (right).

Table 1
MAD X-ray data-collection statistics for the tetragonal crystal form.

Values in parentheses are for the highest resolution shell.

Data set	Peak	High remote	Low remote	Inflection
Wavelength (Å)	0.9797	0.9770	0.9832	0.9799
Unit-cell parameters (Å)	a = 65.5, c = 153.0			
Space group	$P4_12_12$			
Wilson B value (Å^2)	92			
Mean $\lvert E^2 - 1\rvert$	0.80			
Resolution range (Å)	49.8–2.9 (3.0–2.9)	29.5–2.9 (3.0–2.9)	29.5–2.6 (2.7–2.6)	29.5–2.9 (3.0–2.9)
Unique reflections†	13014	13443	19299	13037
Completeness† (%)	92.5 (61.4)	94.6 (71.8)	99.0 (92.8)	92.0 (64.8)
Multiplicity†	6.2 (1.9)	6.5 (3.0)	8.3 (3.9)	6.5 (2.4)
Mean $I/\sigma(I)$†	21.7 (1.9)	22.6 (2.9)	24.4 (2.8)	22.2 (2.3)
$R_{\rm meas}$ ‡	0.078 (0.620)	0.063 (0.635)	0.082 (0.805)	0.057 (0.660)

† For anomalous data. ‡ The redundancy-independent R factor on intensities $R_{\rm meas}$ was calculated according to Diederichs & Karplus (1997).

(Stratagene) and protein production in LB medium was induced at an OD_{600} of 0.4 with 0.1 mM IPTG for 4 h at 303 K. Similarly, the plasmid coding for Hera_208–419 was transformed into *E. coli* BL21 (DE3) Rosetta (Stratagene) and protein production was performed in autoinducing medium (Studier, 2005). Cells were harvested by centrifugation, resuspended in 50 mM Tris–HCl pH 7.5, 100 mM NaCl, 0.1 mM PMSF and disintegrated in a fluidizer (Microfluidics). The supernatant after centrifugation was discarded and the pellet was extracted with 50 mM Tris–HCl pH 7.5, 1 M NaCl. The Hera constructs were precipitated from the supernatant by the addition of 80%(*w*/*v*) ammonium sulfate and were redissolved in 50 mM Tris–HCl pH 7.5, 500 mM NaCl. Dialysis against 50 mM Tris–HCl pH 7.5, 200 mM NaCl, 4 M urea was followed by anion-exchange chromatography on Q-Sepharose in the dialysis buffer to remove nucleic acids. The flowthrough was precipitated with 60%(*w*/*v*) ammonium sulfate and the pellet was dissolved in 20 mM HEPES–NaOH pH 7.4, 500 mM NaCl for gel-permeation chromatography on Superdex-200 (GE Healthcare) in the same buffer. The proteins were concentrated to 5–15 mg ml^{-1} by ultrafiltration. Production of the selenomethionine-substituted protein was performed in minimal medium supplemented with amino acids and it was purified identically to the unsubstituted protein. Generation of the Hera_208–510 triple mutant L272M, L281M, L315M was performed using site-directed mutagenesis (QuikChange, Stratagene).

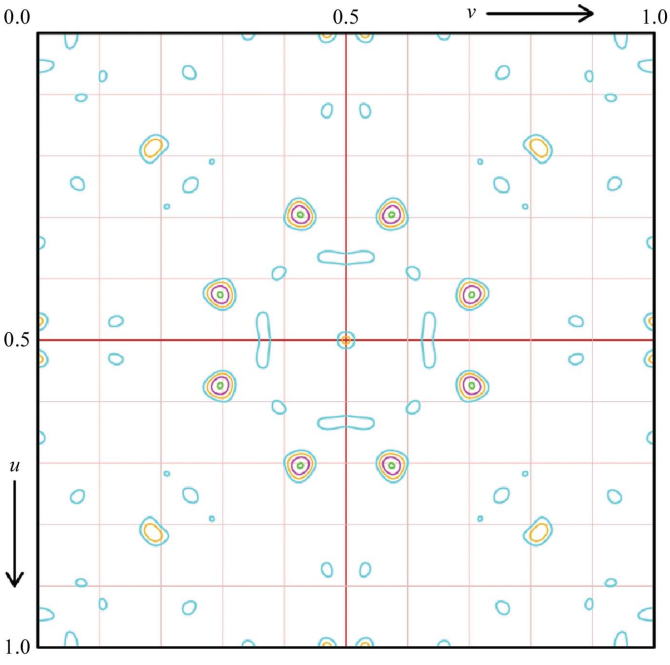

Figure 2
Anomalous difference Patterson map at section w = 0.25 calculated to a resolution of 3 Å showing the single peak at u = 0.42, v = 0.30 for SeMet242 with fractional coordinates (0.776, 0.138, 0.116). Contours are in steps of 1σ and are coloured differently for each level.

Initial crystallization conditions for Hera_208–510 were obtained from Crystal Screen (Hampton Research) using vapour diffusion and were refined using the microbatch-under-oil setup. 9.3 mg ml^{-1} protein in 20 mM HEPES–NaOH pH 7.4, 500 mM NaCl was mixed in a 1:2 volume ratio with precipitant consisting of 0.1 M MES–NaOH pH 6.5, 15–18% ethylene glycol, 0.3–0.5 M NaI, 3–6% PEG 20 000. The final drop volumes were varied from 2 to 6 µl as an additional parameter, with larger drop volumes typically resulting in larger crystals. Tetragonal bipyramidal crystals appeared after 1–4 d at 277 K (Fig. 1*a*). Two rhomboid-shaped crystal forms of Hera_208–419 were obtained using the Index I Screen (Hampton Research). These conditions were refined in the microbatch-under-oil setup at 293 K by mixing 10 mg ml^{-1} protein with precipitant in a 1:2 volume ratio. One form was obtained from 0.1 M Tris–HCl pH 8.5, 0.2 M ammonium sulfate, 23% PEG 3350 (Fig. 1*b*), while another form grew from 0.1 M Tris–HCl pH 7.0, 0.2 M ammonium sulfate, 25% PEG 3350, 5–10%(*w*/*v*) glucose or sucrose (Fig. 1*c*).

2.2. Data collection and analysis

Crystals were initially obtained by vapour diffusion but grew very rapidly, sometimes within a matter of seconds after setup, and did not diffract X-rays beyond 4 Å resolution. Crystals from microbatch under oil grew much more slowly and tended to exhibit better order as judged by X-ray diffraction. Crystals were cryoprotected by replacing the oil from the microbatch experiment with dry paraffin oil, dragging the crystal through the oil layer using a loop and hyperquenching in liquid nitrogen (Warkentin *et al.*, 2006). Cystals were mounted in an arbitrary orientation and data were collected on BESSY beamline BL-1 using a MAR CCD detector (tetragonal form) and on SLS beamline X06SA using a PILATUS detector (orthorhombic forms). Data reduction of the tetragonal crystal form was performed with the *HKL* suite of programs (Otwinowski & Minor, 1997) and data from the orthorhombic forms were integrated with *XDS* (Kabsch, 1993) and scaled with *SADABS* (Bruker). Data statistics for the tetragonal MAD data sets and the native orthorhombic data sets are collected in Tables 1 and 2, respectively. Indexing of the diffraction pattern of the tetragonal crystals was consistent with a primitive lattice of Laue group 4/*mmm* containing one molecule per asymmetric unit (Fig. 1*d*). Analysis of the

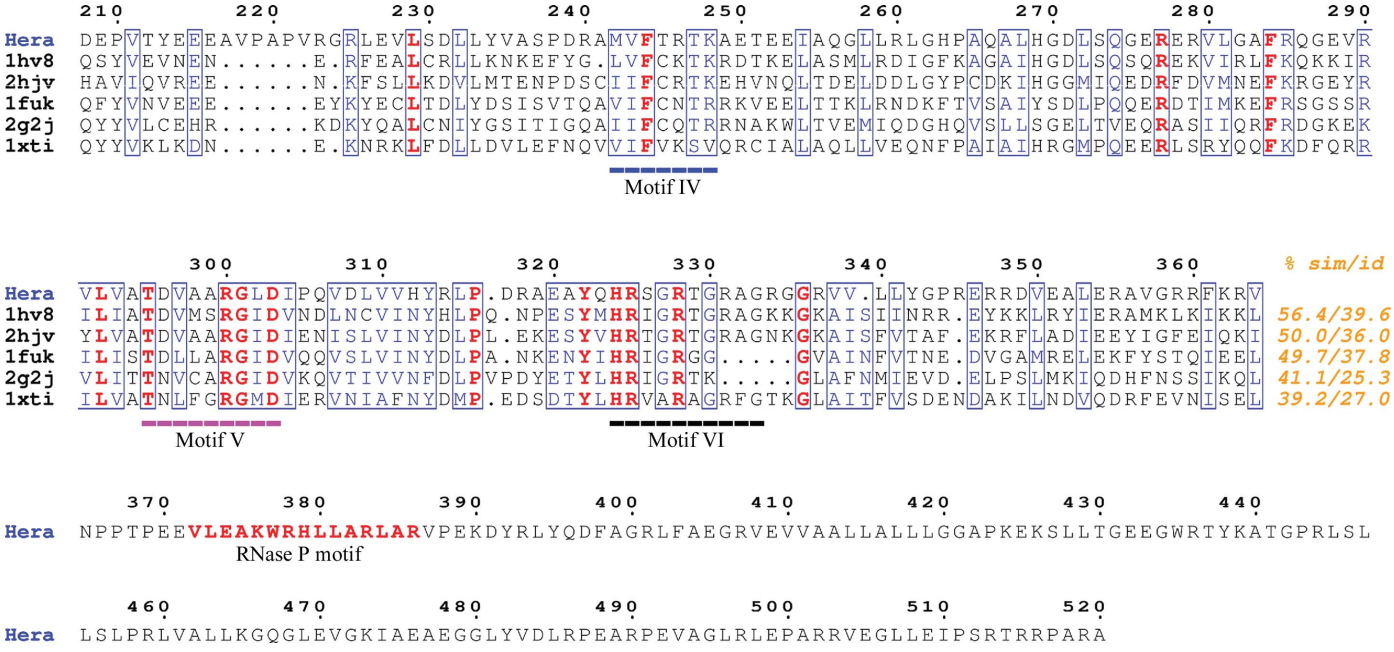

Figure 3
Multiple sequence alignment of C-terminal RecA-like domains from related RNA helicases with Hera_208–510. Conserved residues are in bold, similar residues are boxed and helicase signature motifs as defined in Linder (2006) are underlined. The percentage similarity and identity for the displayed sequence region are given at the end of the alignment. The sequences are labelled with their PDB codes. 1hv8, *M. jannaschii* RNA helicase (Story *et al.*, 2001); 2hjv, *B. subtilis* YxiN (Caruthers *et al.*, 2006); 1fuk, yeast initiation factor 4A (Caruthers *et al.*, 2000); 2g2j, human DDX25 RNA helicase (L. Lehtio *et al.*, unpublished work); 1xti, human UAP56 (Shi *et al.*, 2004). None of these structures proved useful as a molecular-replacement model. The figure was created using *ESPript* (Gouet *et al.*, 2003).

Table 2
X-ray data-collection statistics for the orthorhombic crystal forms.

Values in parentheses are for data in the highest resolution shell.

Data set	Form I	Form II
Wavelength (Å)	1.0	1.0
Space group	$P2_12_12_1$	$P2_12_12_1$
Unit-cell parameters (Å)	a = 62.8, b = 70.9, c = 102.3	a = 41.6, b = 67.6, c = 183.5
Matthews coefficient (Å^3 Da^{-1})	2.42	2.75
Solvent content (%)	49.3	55.2
Wilson B value (Å^2)	58	46
Mean $\lvert E^2 - 1\rvert$	0.80	0.93
Resolution range (Å)	47.0–2.6 (2.78–2.60)	45.9–2.24 (2.38–2.24)
Unique reflections	17245 (2026)	25476 (2630)
Completeness (%)	93.4 (77.8)	87.1 (64.6)
Multiplicity	6.4 (6.6)	6.0 (4.5)
Mean $I/\sigma(I)$	17.6 (2.6)	21.7 (2.4)
$R_{\rm meas}$	0.075 (0.778)	0.045 (0.593)

systematic absences allowed space group $P4_12_12$ or its enantiomorph. The diffraction patterns of the orthorhombic crystals (Figs. 1*e* and 1*f*) indexed in a primitive lattice. Systematically absent reflections established the space group as $P2_12_12_1$ in both cases but with different unit-cell parameters. There are two molecules per asymmetric unit in the orthorhombic crystal forms.

3. Results and discussion

3.1. Phasing using MAD on a single selenium site

An anomalous difference Patterson map at Harker section $w = 0.25$ calculated to 3 Å resolution showed a significant peak of $>5\sigma$, indicating successful SeMet substitution (Fig. 2). The substructure consisting of a single selenium site was determined with *SOLVE* (Terwilliger & Berendzen, 1999). This solution displayed an overall figure of merit (FOM) of 0.34 at 2.9 Å resolution but did not result in an interpretable electron-density map.

In order to improve the experimental phases, two main strategies were pursued: the exploitation of spurious anomalous signal from halide ions and the incorporation of further Se sites by site-directed mutagenesis. The presence of iodide in the crystallization mother liquor (calculated $f' = -2.3$ e$^-$, $f'' = 3.1$ e$^-$ at the peak wavelength) could in principle allow a mixed Se/I substructure. Searches using *SOLVE* or *SHELXD* (Sheldrick, 2008) did not result in additional sites, although substructures of different chemical composition have previously been used for phasing (Roeser *et al.*, 2005). In contrast, crystals containing high concentrations of iodide exhibited severe radiation damage, with the crystals turning red after long exposure times, presumably owing to oxidation of iodide to iodine. Substitution of bromide for iodide during crystallization and repetition of the MAD experiment was unsuccessful and radiation damage at the peak wavelengths for Br and Se prevailed. A SIRAS experiment using an iodide data set as a heavy-atom derivative for a bromide data set was also unsuccessful, although the data sets were isomorphous as judged by similar unit-cell parameters (data not shown). Based on multiple sequence alignment of Hera with other DEAD-box helicases (Fig. 3), three leucine residues (272, 281 and 315) in Hera_208–510 were replaced by methionine in order to increase the number of Se atoms in the substructure. However, while the crystallization conditions remained unchanged, these crystals did not diffract X-rays beyond 3.5 Å resolution and did not result in interpretable electron-density maps (data not shown). A strategy combining molecular replacement, using models derived from homologous RNA helicases, with MAD phasing is currently being used.

We thank Anke Henne for providing *T. thermophilus* HB27 genomic DNA, Ines Hertel, Kathrin Gasow and Andreas Schmidt for

technical assistance and the staff at BESSY beamline BL-1 and SLS beamline X06SA for guidance during data collection. We would also like to thank Gérard Bricogne and Clemens Vonrhein for a pre-release of *BUSTER-TNT* and George Sheldrick for a conversion program from *XDS* to *SADABS* reflection-data format. This work was supported by the German Research Foundation (MGR), the VolkswagenStiftung (DK) and the Swiss National Science Foundation (DK).

References

Andersen, C. B., Ballut, L., Johansen, J. S., Chamieh, H., Nielsen, K. H., Oliveira, C. L., Pedersen, J. S., Seraphin, B., Le Hir, H. & Andersen, G. R. (2006). *Science*, **313**, 1968–1972.
Bono, F., Ebert, J., Lorentzen, E. & Conti, E. (2006). *Cell*, **126**, 713–725.
Caruthers, J. M., Hu, Y. & McKay, D. B. (2006). *Acta Cryst.* F**62**, 1191–1195.
Caruthers, J. M., Johnson, E. R. & McKay, D. B. (2000). *Proc. Natl Acad. Sci. USA*, **97**, 13080–13085.
Diederichs, K. & Karplus, P. A. (1997). *Nature Struct. Biol.* **4**, 269–275.
Diges, C. M. & Uhlenbeck, O. C. (2001). *EMBO J.* **20**, 5503–5512.
Gouet, P., Robert, X. & Courcelle, E. (2003). *Nucleic Acids Res.* **31**, 3320–3323.
Halls, C., Mohr, S., Del Campo, M., Yang, Q., Jankowsky, E. & Lambowitz, A. M. (2007). *J. Mol. Biol.* **365**, 835–855.
Huang, H. R., Rowe, C. E., Mohr, S., Jiang, Y., Lambowitz, A. M. & Perlman, P. S. (2005). *Proc. Natl Acad. Sci. USA*, **102**, 163–168.
Kabsch, W. (1993). *J. Appl. Cryst.* **26**, 795–800.
Kossen, K., Karginov, F. V. & Uhlenbeck, O. C. (2002). *J. Mol. Biol.* **324**, 625–636.
Linden, M. H., Hartmann, R. K. & Klostermeier, D. (2008). *Nucleic Acids Res.* **36**, 5800–5811.
Linder, P. (2006). *Nucleic Acids Res.* **34**, 4168–4180.
Mohr, G., Del Campo, M., Mohr, S., Yang, Q., Jia, H., Jankowsky, E. & Lambowitz, A. M. (2008). *J. Mol. Biol.* **375**, 1344–1364.
Morlang, S., Weglohner, W. & Franceschi, F. (1999). *J. Mol. Biol.* **294**, 795–805.
Otwinowski, Z. & Minor, W. (1997). *Methods Enzymol.* **276**, 307–326.
Pyle, A. M. (2008). *Annu. Rev. Biophys.* **37**, 317–336.
Roeser, D., Dickmanns, A., Gasow, K. & Rudolph, M. G. (2005). *Acta Cryst.* D**61**, 1057–1066.
Rudolph, M. G., Heissmann, R., Wittmann, J. G. & Klostermeier, D. (2006). *J. Mol. Biol.* **361**, 731–743.
Sengoku, T., Nureki, O., Nakamura, A., Kobayashi, S. & Yokoyama, S. (2006). *Cell*, **125**, 287–300.
Sheldrick, G. M. (2008). *Acta Cryst.* A**64**, 112–122.
Shi, H., Cordin, O., Minder, C. M., Linder, P. & Xu, R. M. (2004). *Proc. Natl Acad. Sci. USA*, **101**, 17628–17633.
Story, R. M., Li, H. & Abelson, J. N. (2001). *Proc. Natl Acad. Sci. USA*, **98**, 1465–1470.
Studier, F. W. (2005). *Protein Expr. Purif.* **41**, 207–234.
Terwilliger, T. C. (2000). *Acta Cryst.* D**56**, 965–972.
Terwilliger, T. C. & Berendzen, J. (1999). *Acta Cryst.* D**55**, 849–861.
Theissen, B., Karow, A. R., Kohler, J., Gubaev, A. & Klostermeier, D. (2008). *Proc. Natl Acad. Sci. USA*, **105**, 548–553.
Tsu, C. A., Kossen, K. & Uhlenbeck, O. C. (2001). *RNA*, **7**, 702–709.
Wang, S., Hu, Y., Overgaard, M. T., Karginov, F. V., Uhlenbeck, O. C. & McKay, D. B. (2006). *RNA*, **12**, 959–967.
Warkentin, M., Berejnov, V., Husseini, N. S. & Thorne, R. E. (2006). *J. Appl. Cryst.* **39**, 805–811.